JMEPEG (2010) 19:705–713
DOI: 10.1007/s11665-009-9524-5

1059-9495/$19.00

An Investigation of Strain Concentration in High-Strength Al-Zn-Mg-Cu Alloy 7085 Subjected to Tensile Deformation

C.C. Menzemer, D.F. Lam, and T.S. Srivatsan

(Submitted April 6, 2009; in revised form June 19, 2009)

The strain concentration factors were determined for aluminum alloy 7085 in the T7651 temper using multi-hole structural coupon specimens. Samples of the alloy were evaluated for both the 6.25 mm (0.25 in.) thick and 10 mm (0.4 in.) thick specimens having widths of 50 mm (2 in.) and 100 mm (4 in.), respectively. For the case of the specimens that were 50 mm in width, the mechanical tests were conducted for both the open-hole and filled-hole conditions and the corresponding strain concentration value was determined. For the filled-hole test specimens, threaded fasteners having collars were used. In order to provide for some interference, the fasteners had a shank diameter that was slightly larger than the nominal hole size. The strain concentration values were evaluated at both the failure strain (ε_f) and the strain at maximum load (ε_{max}). The average strain concentration value was then used to predict the results for the stack-up tests.

Keywords aluminum, failure analysis, mechanical testing

1. Introduction

In recent years, several advanced alloys of aluminum have been developed and commercialized. These alloys offer noticeable improvements in intrinsic fatigue crack nucleation and fatigue crack growth resistance coupled with increased strength and toughness as compared to incumbent alloys (Ref 1). However, when these aluminum alloys are tested in a realistic manner relevant to structures, such as in a joint connection test, the effective improvement in strengthened endurance is not as noticeable or large (Ref 2). Through the years, conventional tests make use of a simple one-piece specimen to establish the strength, fatigue life and cyclic resistance of the specific aluminum alloy. In this situation, the crack usually nucleates at one of the larger microstructural heterogeneities in the microstructure such as a constituent particle, a fine microscopic pore or void. However, when the same alloy is tested in a joint and/or structural configuration, the situation becomes complex with additional factors contributing to the 'quality' of the test specimen. Typically, failure is associated with the structural detail representing a stress concentration condition. In a typical aerospace joint, the overall condition of the test specimen depends on the quality of the following interactive and interrelated factors (Ref 2):

(i) Machining to include the production of fastener holes and surface finish of the hole bore.
(ii) Surface quality and treatment to include anodizing and priming.
(iii) Specimen assembly to include alignment, fastener type, fit of the fastener and type of joint and preload force of clamping.
(iv) Amount or extent of fretting between the surfaces of the plates and between the fastener and the plate.

Mechanically fastened joints have become a common feature used by airframe manufacturers and are often considered to be a critical detail in metallic aerospace structures. In many instances, the covering or "skin" of the aircraft is a different alloy than the members making up the skeleton. The optimization of alloy combination requires tests with relevant structural details, in this case, fastener holes coupled with a relevant analysis method. The ultimate acceptance of an aerospace structure that is made from the new and emerging aluminum alloys and the related advanced structural systems is largely dependent upon a successful demonstration of consistent, reliable and predictable performance of the structure while in service. This requirement has necessitated the need for novel methods, spanning the domains of experimental and analytical that can accurately predict the strength, redundancy and durability of these systems while concurrently meeting developmental deadline.

Tension-dominated loading and resultant mechanical behavior is an important consideration in the design, load carrying capability, and overall assessment of stiffened shells. Presently, a vast majority of the structures, spanning the domains of both critical and non-performance critical, used in the aerospace sector make use of mechanical fasteners to either connect or assemble the various components. Testing new design concepts and aluminum alloy combinations for a large aerospace structural system is often tedious, time consuming and taxing by way of expense or cost incurred. Use of simplified tests coupled with judicious use of the principles of solid mechanics to both effectively predict and measurably assess the tensile capacity of skin and stringer combinations prior to committing

C.C. Menzemer and **D.F. Lam**, Department of Civil Engineering, University of Akron, Akron, OH 44324; and **T.S. Srivatsan**, Department of Mechanical Engineering, University of Akron, Akron, OH 44324. Contact e-mail: tsrivatsan@uakron.edu.

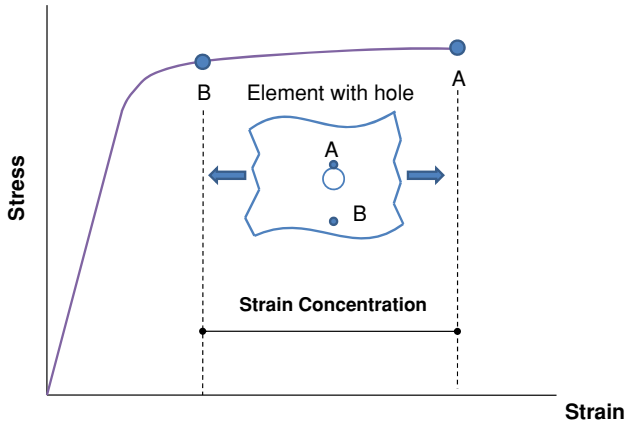

Fig. 1 The strain concentration factor concept

Fig. 2 An aerospace structure that utilizes mechanical fasteners, holes are employed

to full-scale structural simulations is of importance in controlling costs while concurrently meeting developmental deadlines.

The basic premise behind an analysis method that utilizes strain concentration factors for predicting the tensile capacity of a built-up structure views the surrounding material to be subject to strains that are significantly lower than in the immediate area that is either adjacent or local to the fastener (Ref 3). Failure normally initiates at the edge of a fastener hole when the local strain reaches a critical value that is characteristic of what the chosen material can support. The intrinsic differences between the "bulk" strain and the "local" strain are best provided by a direct comparison of results from tests conducted on standard tension specimens and structural coupons having fastener holes. The strain concentration factor concept is illustrated in Fig. 1.

An effective and prudent approach for the determination of strain concentration factor involves mechanical tests that are carefully performed at the level of the material and the structural coupon. Standard material tests were used to evaluate the stress versus strain response up until failure. The structural coupon samples are subsequently tested to provide the stress versus strain characteristics in the presence of relevant engineering detail. For those aerospace structures that make use of mechanical fasteners, holes were employed and a typical sample is shown in Fig. 2. The strain concentration factor is

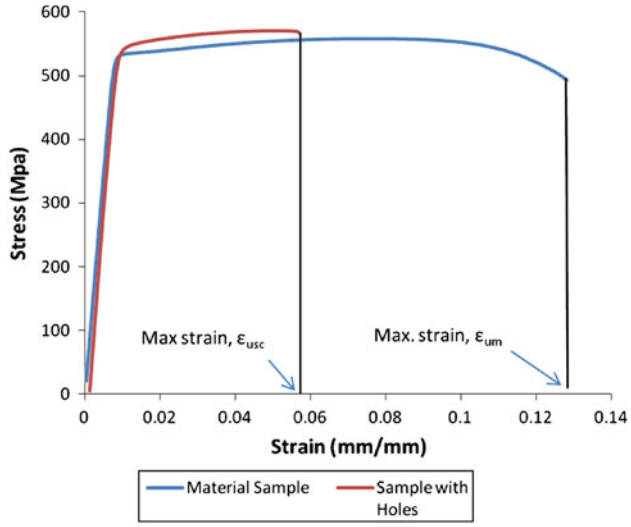

Fig. 3 The determination of the strain concentration factor from mechanical tests

Table 1 Summary of structural coupon samples tested on alloy 7085-T7651

Number	Sample type	Width, mm	Thickness, mm	Number of replicates
1	Open hole	50	6.25	2
2	Open hole	50	10	2
3	Filled hole	50	6.25	2
4	Filled hole	50	10	2
5	Open hole	100	6.25	2
6	Open hole	100	10	2

best rationalized as the ratio of the strain at failure for the material to the strain at failure for the structural coupon. Alternatively, the characteristic strains can also be obtained at the point of maximum load. Typical stress versus strain curves obtained from the mechanical tests are shown in Fig. 3.

The objective of this research paper is to present and discuss the refinement in methodology used for determining strain concentration factors for stiffened aerospace structures made from aluminum alloy 7085-T7651. The strain concentration factor values were determined both at strain at failure (ε_f) and the strain at maximum load (ε_{max}). The experimental test results are used to calculate the strength of the stack-up specimens that are intended to represent a built-up skin-stringer structure. Table 1 summarizes the specimens tested for the chosen aluminum alloy 7085-T7651.

2. Material

The 7000 (7XXX) series aluminum-copper-magnesium-zinc alloys, such as existing aluminum alloys 7085 and 7050, are candidates that are preferred for use in aerospace applications because of the combination of high strength and toughness, along with very low sensitivity to gage length and thickness (Ref 4). The strength is ascribed to the precipitation and presence of strengthening precipitates, $Mg(Zn,Cu,Al)_2$, both

Table 2 Nominal chemical composition of aluminum alloy 7085 (in %)

Element:	Si	Fe	Cu	Mn	Mg	Zn	Ti	Cr	Al
	< 0.06	0.08	1.3	0.04	1.2	7.0	0.06	0.04	Balance

within the grain and along the grain boundaries, and Al_7Cu_2Fe constituent particles (Ref 4). To meet the continuing demand for stronger and tougher aluminum alloys coupled with an attempt to both enhance strength and toughness and enabling an improvement in the safety of existing airplanes, spanning both the military and commercial sectors, a new Al-Cu-Mg-Zn alloy was developed and put forth by ALCOA (Aluminum Company of America) (Ref 5) and was subsequently designated by the Aluminum Association (Washington DC, USA) as 7085. This new alloy was essentially based on aluminum alloy 7050.

The nominal chemical composition of the alloy is given in Table 2. Compared to the incumbent aluminum alloy 7050, alloy 7085 has lower levels of iron (Fe), silicon (Si), and copper (Cu), but contains a small amount of chromium (Cr) and titanium (Ti). The alloy was provided in the T7651 temper, which essentially includes a solution heat treatment, water quench, and a stretch of 1-3% followed by overaging.

3. Test Specimens

The material, i.e., aluminum alloy 7085, was provided by the manufacturer ALCOA as specimen blanks, in some cases milled to the desired thickness prior to final machining. Blanks of the as-received alloy were placed on a computer-controlled milling machine (type: MAHO) and precision cut to the final dimension. The geometry of the test specimen chosen was a "dog-bone" shape having a single row of holes. The effect of specimen width was meticulously evaluated by testing both the 50 mm (2 in.) wide and 100 mm (4 in.) wide samples containing a single row of seven holes. Also examined was the role of fasteners by testing specimens having open holes as well as specimens having holes filled with an aerospace type of fastener. The structural coupons were evaluated for both the 6.25 mm (0.25 in.) thick and 10 mm (0.4 in.) thick conditions. The intricacies of the test specimen geometry are described in detail elsewhere (Ref 6, 7). The alloy (7085) was provided in the T7651 temper as extrusions that can be used as stringers or stiffeners in aircraft structures. The 7085-T7651 alloy provided was considered to be of commercial quality.

4. Experimental Procedures

4.1 Mechanical Testing

The test specimens were mechanically deformed to failure in uniaxial tension. All of the mechanical tests were conducted on a 1330 kN (300,000 lb) Universal Testing Machine manufactured by Warner-Swasey (UK). The load ranges for the Warner-Swasey machine include the following: (i) 50 kN (12,000 lbs), (ii) 270 kN (60,000 lbs), and (iii) 1330 kN (300,000 lbs). The loads were determined to precision using a calibrated pressure transducer that was positioned on the hydraulic cylinder. The strain was measured using a long gage-length extensometer that was acquired from Epsilon Technology. The extensometer used in this research study was unique for two reasons:

(a) It can be left in place through failure of the test specimen.
(b) Its gage length can be easily changed using a variety of inserts.

Test data were recorded on an ADMET controller and were subsequently down-loaded onto a personal computer ("PC") for purpose of analysis. Wedge action grips were used for all of the test samples with ends less than 100 mm (4 in.) in width. Plate grips were utilized for several samples whose grip ends were greater than 100 mm (4 in.) in width.

The stress versus strain curves or plots for the structural coupons are compared to the stress versus strain behavior of aluminum alloy 7085-T7651. The strain concentration factors were then calculated using either the strain at failure (Eq 1) or the strain at the ultimate (maximum) load (Eq 2).

$$K_f = \frac{\varepsilon_{UM}}{\varepsilon_{USC}} \quad \text{(Eq 1)}$$

where K_f is the strain concentration using the strain-at-failure, ε_{UM} is the failure strain for the material at the point of failure or rupture, and ε_{USC} is the failure strain for the structural coupon at the point of failure or rupture.

$$K_{ML} = \frac{\varepsilon_{MML}}{\varepsilon_{SCML}} \quad \text{(Eq 2)}$$

where K_{ML} is the strain concentration using the strain at maximum load, ε_{MML} is the strain for the material at maximum load, and ε_{SCML} is the strain for the structural coupon at the maximum load.

The strain concentration factors were calculated and compared. The comparisons were made in an attempt to determine and/or establish the intrinsic influence of specimen thickness, presence of fasteners, and the role of specimen width on strain concentration factor. The results put forth for both specimen type and calculation methodology are based on an accuracy of the maximum load prediction for the stack-up sample sequence. A single stack-up tensile specimen was built that comprised several layers that included both the skin and stringer material, fastened together using mechanical fasteners.

4.2 Failure-Damage Analysis

The fracture surfaces of the alloy samples that were deformed and failed in tension loading were carefully examined in a scanning electron microscope to (i) determine the macroscopic fracture mode and (ii) to characterize the fine scale topography and microscopic mechanisms governing tensile fracture. The distinction between the macroscopic mode and microscopic fracture mechanism is based entirely on the magnification level at which the observations are made. The macroscopic mode herein refers to the overall failure, while the microscopic mechanism relates to the local failure process, spanning (i) microvoid formation, (ii) microvoid growth and eventual coalescence, and (iii) the nature, extent and severity of cracking spanning both fine microscopic and macroscopic cracks.

5. Results and Discussion

5.1 Initial Microstructure

In the last few years, few studies have been conducted to ascertain the intrinsic microstructural features of aluminum alloy 7050 and their influence on stress versus strain response as obtained from a simple tension test (Ref 8, 9). The microstructure of the as-provided 7085-T7651 was fully recrystallized, with the recrystallized grains flattened and elongated in the longitudinal direction as a direct consequence of mechanical deformation introduced by the extrusion operation. At higher allowable magnifications of the optical microscope, the coarser second-phase particles, i.e., the insoluble iron-rich intermetallics (Al_7Cu_2Fe), were observed to be randomly distributed through the alloy microstructure. In an earlier study on an alloy having near similar composition, these particles were identified as Al_7Cu_2Fe (Ref 8). Overall this type of particle is intrinsically brittle and is a preferred site for crack nucleation. The Mg $(ZnCuAl)_2$ strengthening precipitates were found decorating the grain boundaries.

5.2 Mechanical Test Results

Table 3 succinctly summarizes all of the strain concentration factors determined for alloy 7085-T7651 for the following conditions:

(a) The 50 mm width and 100 mm width.
(b) Open holes and filled holes.
(c) 6.25 mm thickness and 10 mm thickness.

The strain concentration factors that were found using the failure strains (ε_f) are denoted as K_f, while those determined using the maximum load (ε_{max}) are denoted as K_{ML}. The strain concentration values presented are the average value based on multiple tests.

The effect of specimen width on strain concentration factor of aluminum alloy 7085-T7651 is shown in Fig. 4. The strain concentrations presented in Fig. 4(a) are based on the strain at failure, while those shown in Fig. 4(b) are calculated using the strain at maximum load. For this 7085 aluminum alloy in the temper (T7651), the strain concentration does appear to be sensitive to width of the test specimen for the samples. The 100-mm-wide test specimens provided large strain concentration values when compared to the corresponding 50-mm-wide test specimens. This was consistent for both thicknesses, i.e. 6.25 and 10 mm.

Table 3 Strain concentration factors for aluminum alloy 7085-T7651

Number	Sample type Width/thick/open/filled	K_f	K_{ML}
1	50/6.25 and 10/O and F	2.57	1.74
2	50/6.25/O	2.74	1.83
3	50/6.25/F	2.91	1.91
4	50/10/O	2.36	1.59
5	50/10/F	2.31	1.62
6	100/6.25 and 10/O	3.28	2.09
7	100/6.25/O	3.33	2.12
8	100/10/O	3.24	2.06

The intrinsic influence of fasteners on strain concentration factors for aluminum alloy 7085-T7651 is shown in Fig. 5. A comparison of the test specimens having open hole with those having a threaded fastener revealed that the largest effect occurs

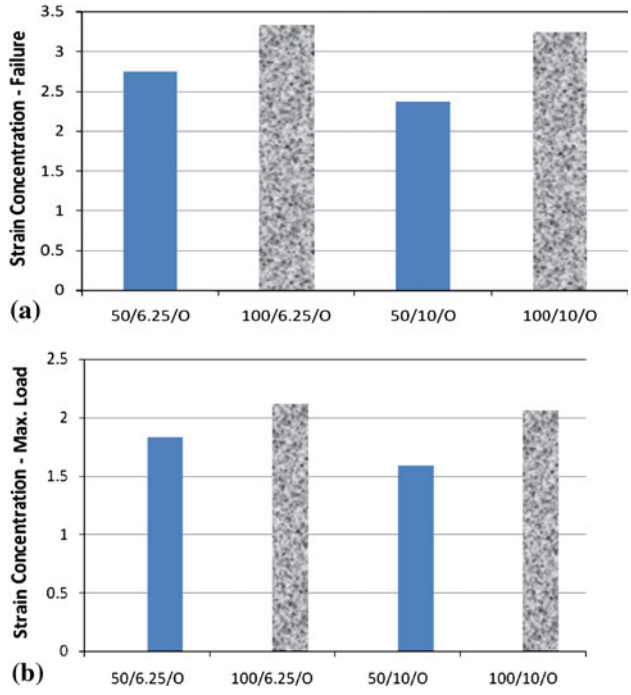

Fig. 4 Effect of specimen width on strain concentration of aluminum alloy 7085-T7651 using (a) failure strains and (b) maximum load

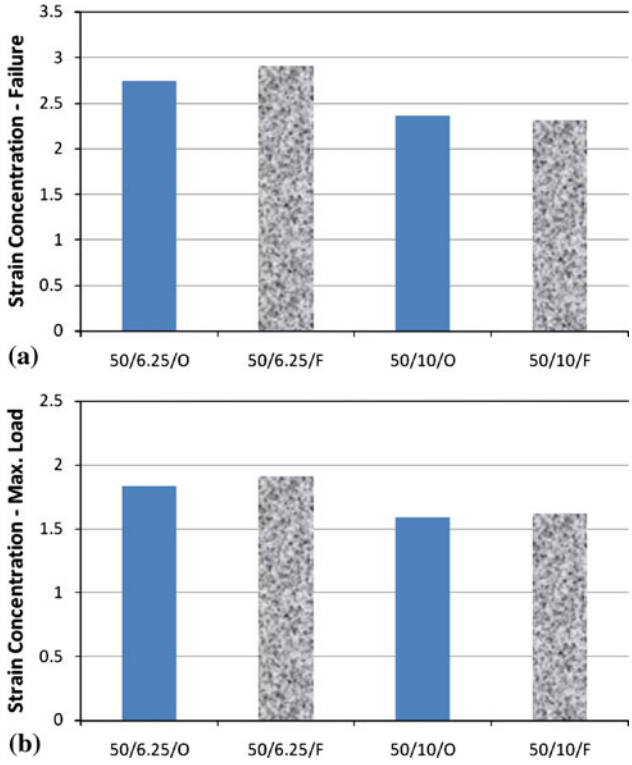

Fig. 5 Effect of fasteners on strain concentration using (a) failure strains and (b) maximum load for 50-mm-wide test specimens of aluminum alloy 7085-T7651

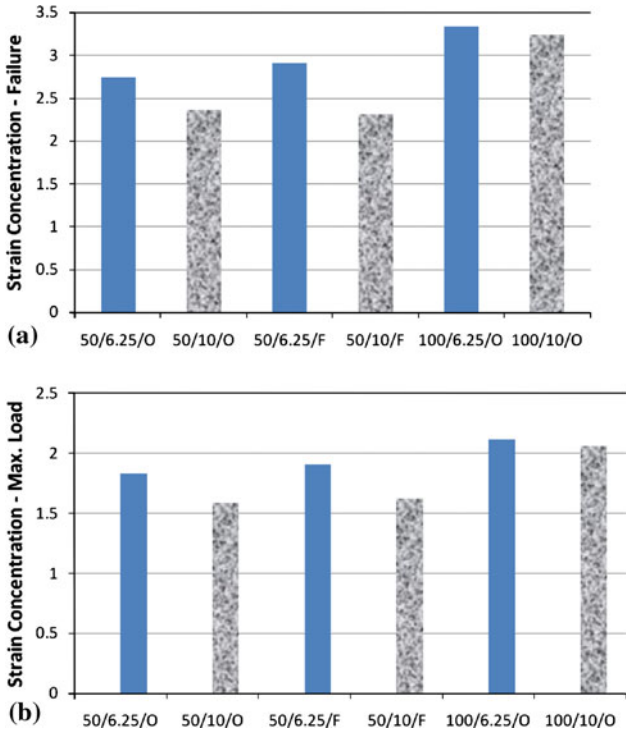

Fig. 6 Effect of sample thickness on strain concentration using (a) failure strain and (b) maximum load for aluminum alloy 7085-T7651

for the 6.25-mm-thick specimens. The 10-mm-thick specimens appeared to have a smaller difference in strain concentration when comparing the open hole with the filled hole specimens.

The influence of test specimen thickness on strain concentration factor for aluminum alloy 7085-T7651 is shown in Fig. 6. The strain concentration factor based on failure strain is shown in Fig. 6(a) while the strain concentration factor based on strain at maximum load is shown in Fig. 6(b). The 10-mm-thick specimens had a noticeably lower strain concentration when compared to the 6.25-mm-thick specimens of the alloy. Also, an increase in specimen width appeared to reduce the extent of the difference in the two strain concentration factors calculated either at the failure strain and maximum load.

A direct comparison of the strain concentration factor data for aluminum alloy 7085-T7651 calculated both at the failure strain (ε_f) and strain at maximum load (ε_{ML}) is shown in Fig. 7. It is observed that for both thicknesses (6.25 and 10 mm) and widths (50 and 100 mm) the strain concentration value based on failure strain is consistently higher than the strain concentration values calculated using the strain at maximum load.

5.3 Tensile Fracture

The tensile fracture surfaces provide useful information on intrinsic microstructural effects on strength, ductility and fracture properties of aluminum alloy 7085-T7651. The scanning electron micrographs of the test samples that were deformed and failed in tension revealed identical macroscopic failure mode regardless of width and thickness of test specimen. However, noticeable differences in the microscopic fracture mode were clearly evident as revealed by the microscopic features on the tensile fracture surface. Representative fracture features of the deformed and failed samples are shown in Fig. 8 and 9.

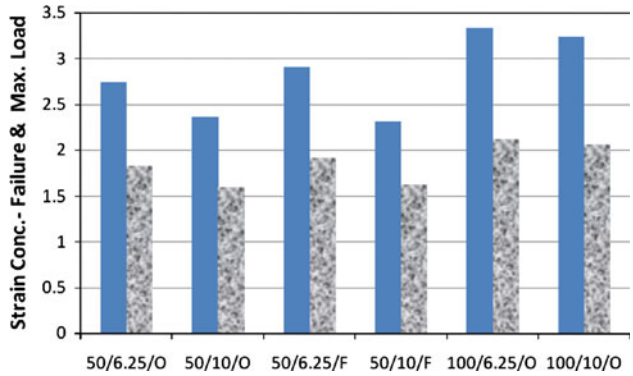

Fig. 7 A comparison of strain concentration of aluminum alloy 7085-T7651 at failure strain and maximum load

At ambient temperature (27 °C) microscopic fracture of the 7085-T7651 alloy was normal to the major stress axis with an overall mixed-mode, i.e., ductile-brittle appearance (Fig. 8a). Fracture was predominantly transgranular with cracking along the recrystallized grain boundaries (Fig. 8a). The transgranular regions were essentially flat and neat featureless (Fig. 8b). Isolated pockets of fine microscopic voids and shallow dimples were evident along the grain boundary regions (Fig. 8b). Higher magnifications in the scanning electron microscope revealed distinct cracking along the high-angle grain boundaries with fine shallow dimples decorating the grain boundary regions (Fig. 8c). The cracking occurred with ease along the grain boundary triple junctions. Coalescence of the fine microscopic voids initiated at the grain boundary precipitates resulted in dimple formation type intergranular fracture. The recrystallized grains were large with distinct cracking along the recrystallized grain boundaries (Fig. 9a) and running parallel to the major stress axis (Fig. 9b). The array of coplanar cracks along with the presence of microscopic voids and dimples along the grain boundary regions suggests that failure of the sample was predominantly intergranular at the microscopic level. This can essentially be attributed to a large area fraction of the weakened high-angle grain boundaries parallel to the longitudinal direction. This intergranular fracture and resultant delamination brings about a loss of through thickness constraint causing an essentially plane strain brittle fracture process to be divided into several plane stress ductile fracture at the microscopic level (Ref 10, 11). The beneficial effect of crack tip plasticity is offset by the presence of intergranular precipitates coupled with coarse constituent particles. These intrinsic microstructural features promote the occurrence of brittle intergranular fracture and cracking of the coarse second-phase particles, i.e., Al_7Cu_2Fe, spread through the alloy microstructure (Fig. 9c). The nucleation, growth and eventual coalescence of the fine microscopic voids initiated at the grain boundary precipitates and particles occur at low to moderate stress levels (Ref 11, 12). The halves of these voids are the shallow dimples covering the intergranular fracture regions (Fig. 9b).

5.4 Model Development

The failure load for the sample having a single line of fasteners was estimated using an idealized stress distribution at failure. This stress distribution is based on a numerical simulation and is shown in Fig. 10. The stress distribution is taken as blocks across the width of the sample. Extending one

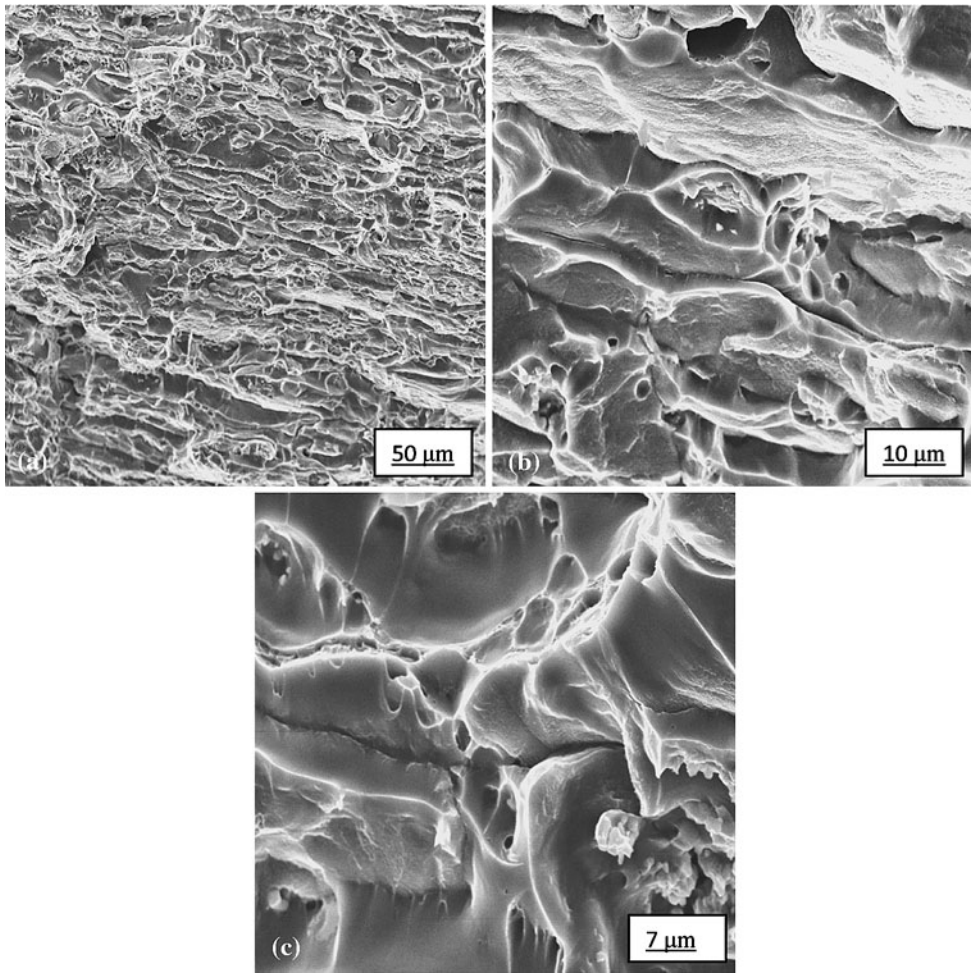

Fig. 8 Scanning electron micrographs of the 7085-T7651 alloy sample deformed in tension, showing the following: (a) overall morphology showing mixed mode, i.e. ductile-brittle failure; (b) array of coplanar cracks along the recrystallized grain boundaries; (c) cracking at grain boundary triple junctions, voids and shallow dimples

diameter on either side of the hole the stress is taken to be equal to the ultimate tensile strength. Immediately adjacent to the ultimate stress, for one full diameter, is a flow like stress, which is taken to be the average of the yield strength and ultimate tensile strength, i.e., $[(\sigma_{YS} + \sigma_{UTS})/2]$. The remainder of the cross section is taken to be at the level of the yield strength of the alloy.

The test results obtained from using the simplified model to predict the failure load for a 50-mm-wide, 6.25-mm-thick specimen is shown in Fig. 11. It is noted that the strength of aluminum alloy 7085-T7651 is taken from the same lot of material as the coupon specimen. Further, the average strength was used for the purpose of prediction and comparison with the failure load obtained from mechanical testing. For purpose of comparison test, data from an emerging aluminum alloy designated as C460-T8E67 and having near similar composition are also provided. The predicted failure load is compared with the structural coupon test results for the 50-mm-wide, 10-mm-thick specimen and is shown in Fig. 12. Figure 13 compares the predicted and experimental test results for the 100-mm-wide, 6.25-mm-thick samples of the emerging aluminum-lithium alloy C460-T8E67 (AA designation 2099) and the established 7085-T7651 alloy having open holes. Results for the 100-mm-wide, 10-mm-thick coupons of the two alloys are compared in Fig. 14. For the cases considered, i.e., sample width and thickness, the predictions were generally well within 5% of the average structural coupon test results for alloy 7085-T7651. A near similar trend was observed for the aluminum-lithium alloy C460 in the T8E67 condition with the predicted load being lower than the test value.

The research personnel at ALCOA Technical Center (Pittsburgh, PA) provided test results from tension tests on built-up samples, referred to henceforth as stack-up samples, comprising outer layers of the skin alloy (7085-T7651) and a single middle layer of the extrusion or stringer alloy (C460-T8E67). Each of the stack-up samples made from the chosen alloys was mechanically deformed in tension until failure. The strain concentration factors determined from the stack-up tests were used to predict the results of the built-up samples using a weighted average stress approach. As put forth in the published literature (Ref 3), the expression put forth for the failure stress of the built sample is given by:

$$\sigma_F = \frac{A_{sn}\sigma_{ts} + A_{en}\sigma_{te}}{A_g}$$

where A_{sn} is the net or effective area of the skin along the failure plane, A_{en} is the net or effective stress of the stringer

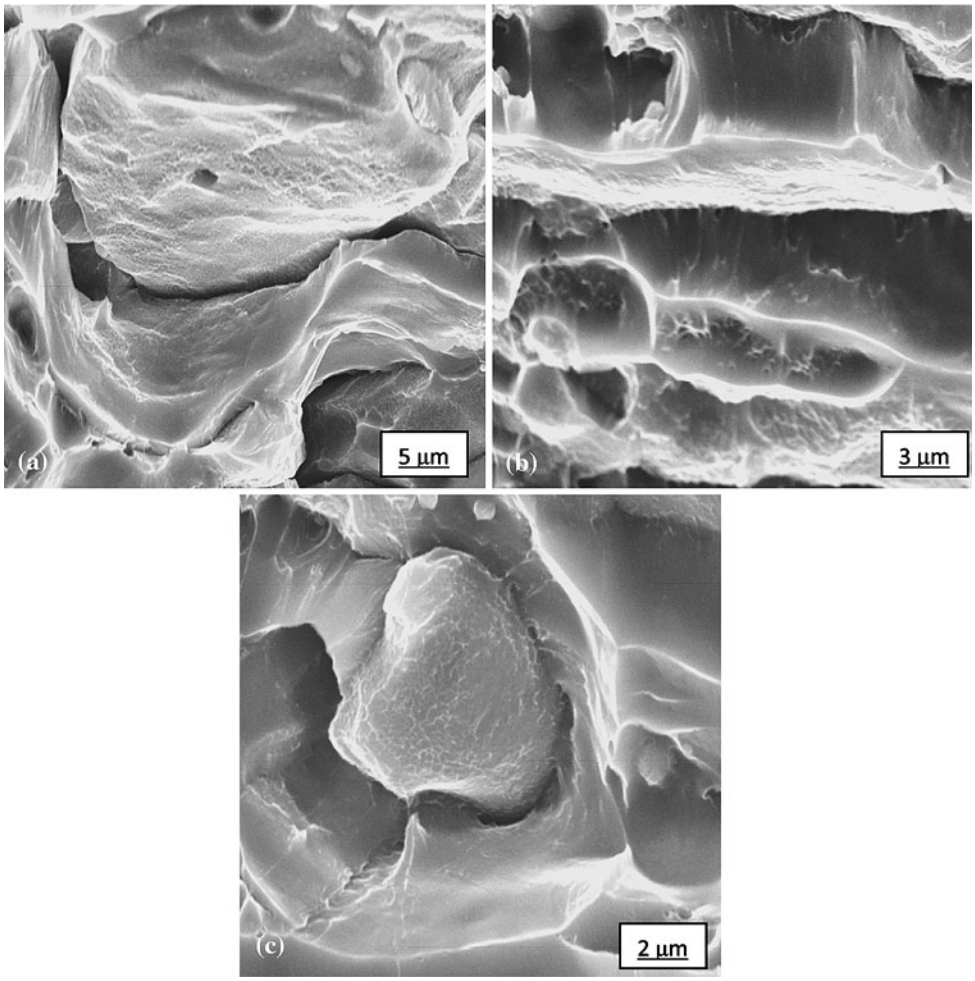

Fig. 9 Scanning electron micrographs of the 7085-T7651 alloy sample deformed in tension, showing the following: (a) cracking at the recrystallized grain boundary; (b) coplanar cracks along the high-angle grain boundaries and near featureless transgranular region; (c) cracking around a coarse second phase constituent particle

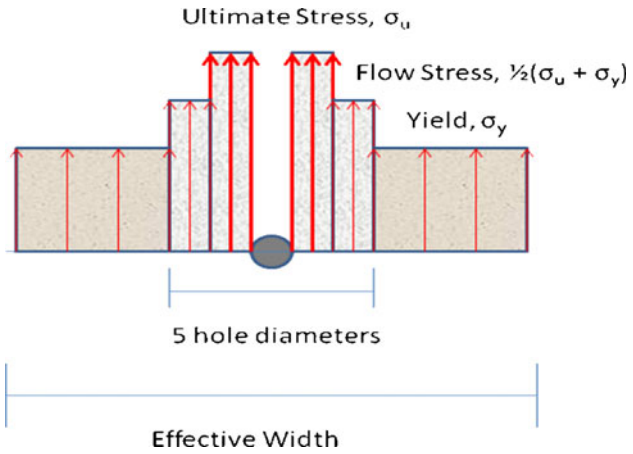

Fig. 10 Assumed stress distribution at failure close to fastener holes

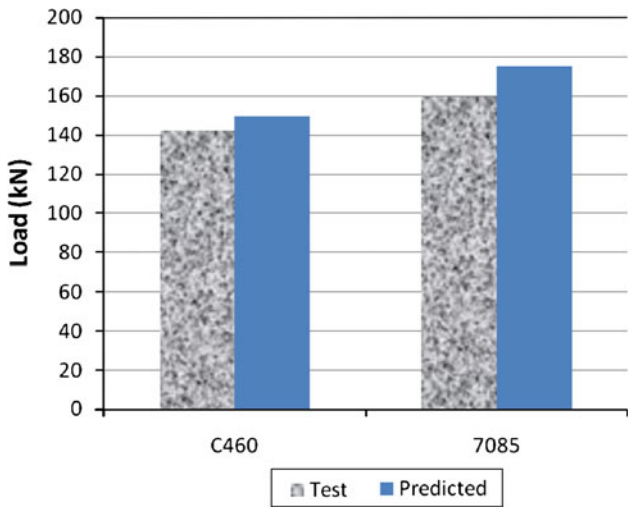

Fig. 11 A comparison of the simplified model and test results for 50-mm-wide, 6.25-mm-thick specimen of aluminum alloy 7085

along the failure plane, σ_{ts} is the net skin stress corresponding to failure strain of the panel and σ_{te} is the net stress in the stringer at failure strain of the panel, A_g is the gross area, and σ_F is the failure stress of the gross area. The numerator of this expression reduces to load (the product of stress times area), which when divided by area provides the failure stress of the structural member.

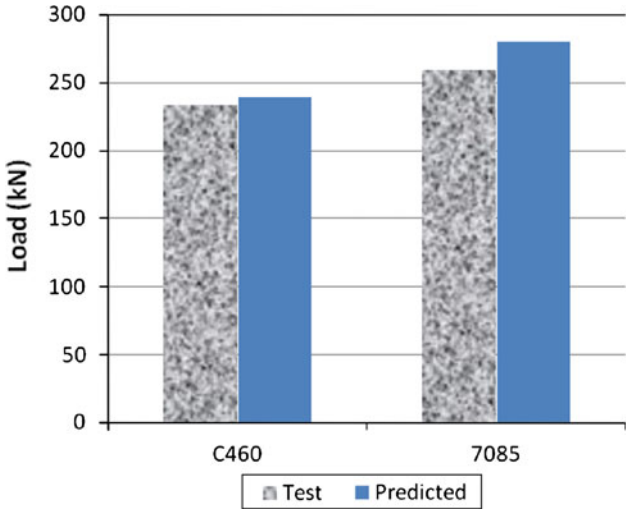

Fig. 12 A comparison of model predictions and test results for the 50-mm-wide, 10-mm-thick specimens of aluminum alloy 7085

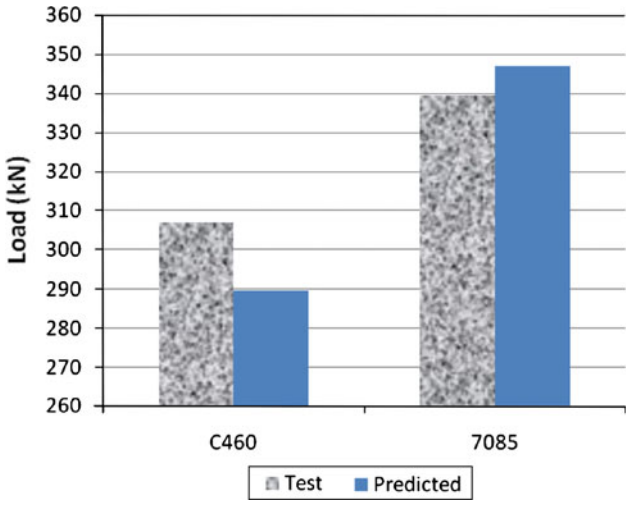

Fig. 13 A comparison of the predicted and test results for the 100-mm-wide, 6.25-mm-thick test specimens of aluminum alloys 7085 and C460 having open holes

A precise determination of the predicted load for the built-up sample starts with plotting the stress versus strain curves for the alloys and a subsequent identification of the critical element. Typically, the critical element is found for the layer whose behavior is limited or constrained by ductility. In other words, when the stack-up specimen layers are firmly connected and acts as a complete unit, then mechanical deformation of the different layers is the same. Failure of the sample is essentially dictated by the layer of the alloy that has a smaller or limited deformation capacity. The strain concentration for the alloy and relevant details, i.e., open-hole and filled-hole, is then applied to the stress versus strain curve of the critical element to determine the ultimate failure strain of the panel. The critical stresses for each element are determined for failure strain of the panel. The gross area panel failure stress [F_t] is then computed.

The results of an estimation of the failure load for the stack up sample are shown in Fig. 15. Besides the independent testing in our laboratory, several sets of data for a combination

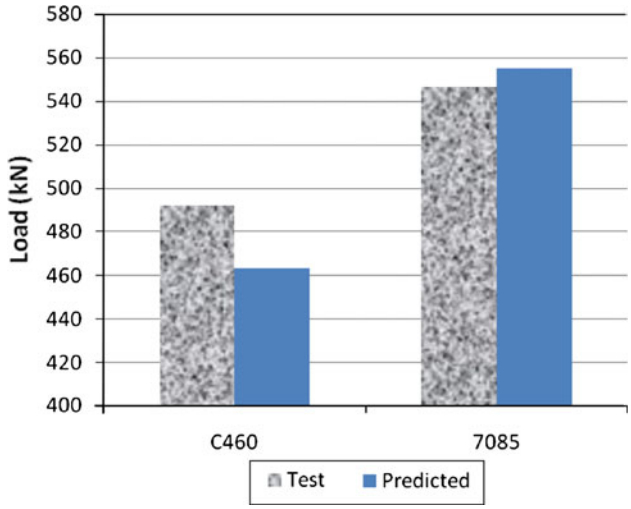

Fig. 14 A comparison of predicted and test results for 100-mm-wide, 10-mm-thick specimens of aluminum alloys 7085 and C460

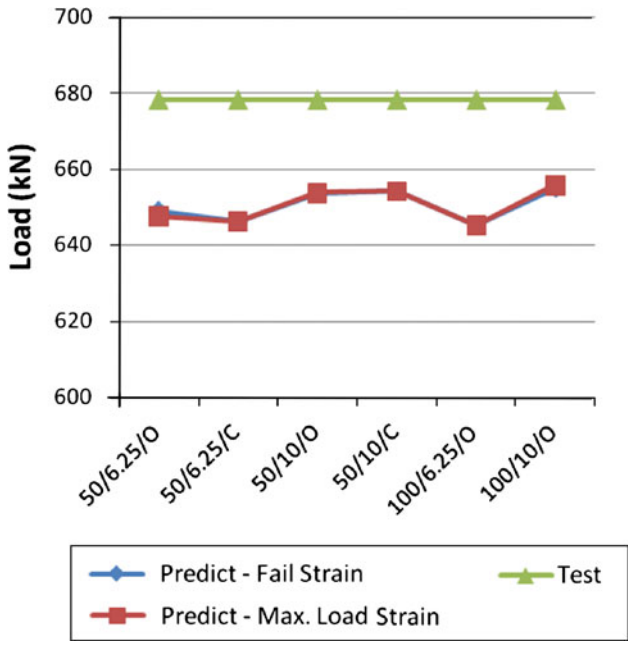

Fig. 15 Exemplification of stack-up test results for alloy C460-7085 combination

of alloys C460 and 7085 were made available by research personnel at Alcoa Technical Center (Pittsburgh, PA, USA). As the thicknesses of the layers were marginally different (example: top layer 7085 is 5.5 mm in thickness, the middle layer is alloy C460 of 9.9 mm thickness and the bottom layer is alloy 7085 of 5.5 mm in thickness), the C460-7085 alloy stack-up combination was treated as an independent unit. For each plot, the predictions utilizing the strain concentration factors at (i) the failure strain and (ii) the maximum load are shown.

An inspection of Fig. 15 reveals that the difference between the average test result and the predicted maximum load varies between 3 and 5%. In order to provide a valid recommendation on the preferred specimen geometry, the experimental data were evaluated by calculating the professional factor, which in this

study is referred to as the ratio of the predicted maximum load to the actual test result obtained for the specific sample configuration chosen as well as definitions of the two strain concentration factors.

6. Conclusions

A series of structural coupon tests were performed with precision on samples fabricated from aluminum alloy 7085-T7651. The tests were conducted on samples having both open holes and filled holes. The filled hole samples utilized a threaded fastener that contained a collar. The test specimen configurations included widths of 50 and 100 mm and thicknesses of 6.25 and 10 mm. The following are the key findings:

1. Strain concentration factors were developed for all the samples tested, utilizing the strain at failure (ε_f) and the strain at maximum load (ε_{ML}).
2. A comparison of the 50-mm-wide and 100-mm-wide samples revealed that an increase in width of the test sample resulted in an increase in strain concentration factor. The presence of a hole should only have a small influence as the width of the test specimen increases since a large portion of the specimen cross-section experiences a significantly smaller strain when the failure initiates at or close to a hole.
3. Filling the holes in the test sample with threaded fasteners resulted in a noticeable increase in strain concentration value for this aluminum alloy 7085-T7651. The increase was particularly noticeable when using the strain at failure. The intrinsic influence of the presence of fasteners is of value in bearing-type connections.
4. Increasing the thickness of the test sample resulted in a concomitant decrease in strain concentration factors for this alloy in the T7651 condition. The effect of thickness can be ascribed to differences in stress distribution from the surface of the test sample to the interior of the test sample particularly adjacent to the hole.
5. The predictions of the failure load for the sample having a single line of fastener were estimated using an idealized stress distribution at failure and were generally well within 5% of the average structural coupon test results. A similar trend was observed for the ternary alloy C460 in the T8E67 condition.
6. The difference between the average test result and the predicted maximum load varied between 3 and 5%.

Acknowledgments

The material used in this exhaustive research study was provided by ALCOA (Aluminum Company of America). Sincere thanks and appreciation is extended to the research personnel at ATC (ALCOA Technical Center) for providing financial support as well as the relevant data required for this research study. Thanks are also extended to the University of Akron for providing tuition support to the graduate student. Finally, the authors extend overwhelming thanks and appreciation to the two unknown reviewers whose comments, corrections and suggestions have helped strengthen the revised manuscript.

References

1. R.T. Shuey, F. Barlat, M.E. Karabin, and D.J. Chakrabarti, Experimental and Analytical Investigations on Plane Strain Toughness for 7085 Aluminum Alloy, *Metall. Mater. Trans. A*, 2009, **40**, p 365–376
2. G.H. Bray, ''Comparison of Open Hole and Joint S/N Fatigue Test Results for Standard and High Purity 7055-T7751 Plate,'' ATC Report 01A56501, Pittsburgh, PA, 1998
3. M. Mohaghegh, Tension Analysis of Stiffened Aircraft Structures, AIAA-85-0795-CT, *26th Annual Joint Conference of AIAA/ASME/ASCE/AHS Structures, Structural Dynamics and Materials Conference*, Orlando, FL, 1985
4. C. Giummara and H.R. Zonker, Improving the Fatigue Response of Aerospace Structural Joints, *ICAF 2005 Proceedings*, Hamburg, Germany, 2005
5. D.J. Chakrabarti, J. Liu, R.R. Sawtell, and G.B. Venema, *Proceedings of ICAA9* (North Melbourne), Institute of Materials Engineering Australasia Ltd., 2004, p 969–974
6. D.F. Lam, ''Strain Concentration and Tension Dominated Stiffened Aerospace Structures,'' Master of Science Thesis, The University of Akron, Akron, OH, May 2006
7. C.C. Menzemer, ''Strain Concentration and Tension Dominated Stiffened Aerospace Structures,'' Final Technical Report to Aluminum Company of America, March 2006
8. T.S. Srivatsan, D. Lanning, Jr., and K. Soni, Cyclic Strain Resistance and Fracture Behavior of High Strength Aluminum Alloy, *J. Mater. Sci*., 1993, **28**, p 3205–3213
9. T.S. Srivatsan, Microstructure, Tensile Properties and Fracture Behavior of Aluminum Alloy 7150, *J. Mater. Sci.*, 1992, **27**, p 4772–4781
10. D. Hoeppner, S. Adibnazari, and M.W. Moesser, ''Literature Review and Preliminary Studies of Fretting and Fretting Fatigue Including Special Applications to Aircraft Joints,'' Report DOT/FAA/CT-93/2
11. E.R. Speakman, Advance Fastener Technology for Composite and Metallic Joints, *Fatigue in Mechanically Fastened Composite and Metallic Joints*, ASTM STP 927, J.M. Potter, Ed. (Philadelphia, PA), American Society for Testing and Materials, 1986, p 5–38
12. T.S. Srivatsan and V.K. Vasudevan, The High Strain Cyclic Fatigue and Fracture Behavior of Two Al-Cu-Mg Alloys, *Met. Mater. Processes*, 1994, **6**(2), p 97–106